Global Modeling of Active Terahertz Plasmonic Devices

Mohammad Ali Khorrami, *Student Member, IEEE*, Samir El-Ghazaly, *Fellow, IEEE*, Hameed Naseem, *Senior Member, IEEE*, and Shui-Qing Yu, *Member, IEEE*

***Abstract*—In this study, a full wave numerical technique is employed to characterize the propagation properties of 2-D plasmons along two-dimensional electron gas (2DEG) layers of biased hetero-structures at terahertz frequencies. This method is based on a coupled solution of Maxwell and hydrodynamic transport equations. In this manner, a complete description of carrier-wave interactions inside the 2DEG layer is obtained. Particularly, this simulator is employed to investigate the 2-D plasmon variations initiated by the application of an external bias along the hetero-structure. Substantial changes in the plasmon characteristics such as wavelength and decay length are reported. It is also revealed that two symmetrical plasmonic modes along the unbiased 2DEG layer split into new asymmetrical ones after applying the bias voltage. The simulation has been performed in different structures to examine the effects of various electron densities and the presence of periodic metallic gratings on the plasmon properties. Moreover, the 2-D plasmon reflections from boundaries terminated by ohmic contacts are separately studied. This research demonstrates the potentials of the 2-D conductors in the design of novel active terahertz plasmonic devices as modulators and amplifiers while proposing a new approach for their modeling. The results of this simulation are verified independently with an analytical model.**

***Index Terms*—Boltzmann transport equation, global modeling, Maxwell equations, plasmonic, terahertz (THz).**

I. Introduction

RECENTLY, there has been a great interest among microwave and photonic research groups to exploit nano-plasmonics both in the visible and terahertz (THz) frequency ranges [1]–[3]. While surface plasmons (SPs) propagating on a dielectric–metal interface are suitable for localizing EM waves in nano-sized dimensions at optical frequencies, they are not confined to the interface at the lower part of the electromagnetic spectrum such as microwave and THz frequencies [4]. Therefore, the application of a highly doped semiconductor instead of the metal [4], engineering the metal electromagnetic (EM) properties by making holes and indentations on its surface to enhance carrier–wave interactions [5], [6], or employing 2-D conductors [7]–[10] have been proposed. Specifically, 2-D conductors have become more interesting after the advent of graphene with very high charge mobilities even at room temperatures [11], [12]. In 2-D conductors, smaller numbers of electrons are affected by the EM waves compared to the metal-dielectric interface. Therefore, the collective plasma mode of the electrons gains significant amount of kinetic energy compared to the energy of the surrounding EM fields even at microwave and THz frequencies [13]. These plasma waves in 2-D conductors are mostly called 2-D plasmons or surface waves coupled to surface carries (shortened as SWC) [14]. They can propagate with velocities far lower than what is observed in SPs. Besides, 2-D plasmon wavelengths can be even 700 times smaller than the radiating mode wavelength in the free space [13]. Hence, 2-D plasmons can be very useful in the fabrication of nano-sized microwave and THz devices. Specifically, 2-D plasmons along the two-dimensional electron gas (2DEG) layers of hetero-structures have been vastly employed in the design and fabrication of sources [15], [16], resonant and non-resonant detectors [17]–[19], crystals and interferometers [13] and switches [20].

Mostly, the analysis of passive 2-D plasmonic devices is performed using EM simulators as finite difference time domain (FDTD) [21] or distributed lumped element models [22]. These simulators represent conductors and doped semiconductors with the aid of Drude model as calculating field distributions and mode profiles within the devices. However, the analysis of modern active plasmonic circuits and devices as sources and detectors is not possible by simply using Drude model. This limitation exists since Drude approximation is a zero-bias voltage model. Therefore, variations of the EM wave characteristic originated from the moving electrons accelerated by applied electric fields are disregarded. Besides, this model does not consider complex electron distributions inside the devices. Therefore, it is not able to provide a complete picture of electron–wave interactions. Nonlinear effects such as electron velocity saturation due to electron heating are also not taken into account with this approximation. Previously, several analytical [8] and [23], and numerical [24] solutions of Possion equation have been proposed to describe the THz wave propagation inside the 2-D conductors. However, Poisson equation is not able to provide a fundamental insight into the electromagnetic wave propagation inside complex modern active plasmonic devices. For instance, wave impedances and transmitted power of each plasmonic mode is completely unknown while approximating the wave propagation using Poisson equation.

The rise of the active plasmonic area requires the development of a full wave simulator which enables the designer to completely capture the underlying physics of these devices. This simulator must provide a complete solution of coupled Maxwell and electronic transport equations. Previously, the necessity to characterize the carrier-wave interactions inside

Manuscript received April 22, 2013; revised August 04, 2013; accepted August 30, 2013. Date of publication September 30, 2013; date of current version January 17, 2014.

The authors are with Department of Electrical Engineering, University of Arkansas, Fayetteville, AR 72701 USA (e-mail: mkhorram@email.uark.edu).

Color versions of one or more figures in this paper are available online at http://ieeexplore.ieee.org.

Digital Object Identifier 10.1109/TTHZ.2013.2281146

microwave transistors has led to the development of a similar numerical solver, mostly called global modeling [25], [26]. Global modeling has also been employed at THz frequencies to characterize the electrical conductivities of silicon [27] and graphene layers [28]. In spite of the application of this modeling method in different high frequency applications, it has not been previously employed in the plasmonic area.

In this paper, we have employed the in-house global modeling simulator [25], [26] to characterize the 2-D plasmon propagation inside a non-degenerate 2DEG layer of a hetero-structure. This solver has been already validated through comparison of small-signal parameters and output voltages of similar microwave transistors with experimental results. This simulator solves a set of conservation equations, developed from the moments of Boltzmann transport equation, and Maxwell equations self-consistently. Here, global modeling is employed to investigate the possibility of guiding and amplifying THz plasmons in the 2DEG layer by applying a bias electric field. It is shown that the plasmon properties change vastly as the electrons are accelerated by the bias field. This type of investigation is able to provide real time information about electron density and velocity inside the plasmonic channel. In order to verify the results, the analytical model developed in [29], [30] is employed. Compared to the analytical model in [29], [30], this full wave simulator is able to consider the finite thicknesses of electron gas layers. Additionally, the influence of the wide band-gap semiconductor thickness on the properties of the 2-D plasmons can be investigated. Moreover, the presence of ohmic contacts on the propagation characteristics of the surface waves can be examined using the global modeling method. Furthermore, the presence of metallic gratings, mostly fabricated on the device surface to excite a specific plasmonic mode may be taken into account using this technique.

The paper is organized as follows. In Section II, an overview of the numerical scheme previously developed in [25], [26] is presented while required changes to simulate the plasmonic structures are described. In Section III, the solver is utilized to characterize 2-D plasmon propagation inside a 2DEG layer of a hetero-structure under different biased voltages. Moreover, the wave reflections from ohmic contacts are considered in this section to present the superior capabilities of the numerical technique in comparison to the analytical model. Section IV describes the effects of changing the charge densities of the 2DEG layer and the presence of a periodic metallic grating located at the device surface on the SWC properties.

II. Models and Methods

A. Electronic Transport Model

Electron dynamics inside 2DEG layers of hetero-structures can be described by solving the moments of Boltzmann transport equation [25]. These strongly coupled highly nonlinear set of partial differential equations relating volume electron density n_v and electron momentum $\vec{p}$ are

1) Complete Form of Momentum Conservation:

$$\frac{\partial(n_v p_x)}{\partial t} + \nabla \cdot (n_v p_x \vec{v}) + \frac{\partial}{\partial x}(n_v k_B T) = q n_v (E_x + (\vec{v} \times \vec{B})_x) - \frac{n_v p_x}{\tau_m}. \quad (1)$$

2) Continuity Equations:

$$\frac{\partial n_v}{\partial t} + \nabla \cdot (n_v \vec{v}) = 0 \quad (2)$$

where q, τ_m, T, and $\vec{v}$ are electron—unit charge, momentum relaxation time, temperature, and velocity, respectively. Moreover, k_B, $\vec{B}$ and $\vec{E}$ are Boltzmann constant, the magnetic flux and the electric field at the electron position, respectively. Additionally, the momentum conservation equation (1) can be similarly rewritten in other directions (y and z) too. Electronic current density $\vec{J}_v$ inside the 2DEG may be calculated at any time t as $\vec{J}_v(t) = -q n_v(t) \vec{v}(t)$. Furthermore, the electron momentum and velocity are related through the electron effective mass m^* ($p = m^* \times v$). In general, a complete 1-D solution of the transport (continuity, momentum and energy conservations) equations can be performed. However, energy conservation equation (not mentioned here) is not included in the solution presented in this paper. This does not change the validity of our analysis since the bias voltage and the ac incident electric fields are both chosen such that the device operates only in the linear section of the electron velocity-electric field curve [31].

B. Electromagnetic Model

Maxwell equations can accurately characterize electromagnetic field propagation. In a uniform, isotropic and linear medium with relative permittivity ε_r and permeability μ_r, Maxwell equations are

$$\nabla \times \vec{H} = \varepsilon \frac{\partial \vec{E}}{\partial t} + \vec{J}_v \quad (3)$$

$$\nabla \times \vec{E} = -\mu \frac{\partial \vec{H}}{\partial t}. \quad (4)$$

In (3)–(4), $\vec{H} = \vec{B}/\mu$, $\varepsilon = \varepsilon_0 \times \varepsilon_r$ ($\varepsilon_0 \approx 8.85 \times 10^{-12}$ F/m) and $\mu = \mu_0 \times \mu_r$ ($\mu_0 \approx 4\pi \times 10^{-7}$ H/m) are the magnetic field and the permittivity and the permeability of the corresponding medium, respectively. FDTD is a time domain solution of Maxwell equations using a mesh where the field components are arranged inside following Yee scheme [32]. The time and space derivatives in (3) and (4) are estimated using central differencing with the second-order accuracy.

C. Coupling the EM and the Electronic Transport Model

The EM solver calculates the field variations due to the moving charges while the electronic transport simulator updates charge properties altered by the applied fields. By passing physical parameters such as the fields and the current density between the two models, an appropriate link is established among the simulators. The initial state of the time-dependent calculation is obtained by solving Poisson equation ($\nabla^2 V = -q[N_D^+ - n_v]/\varepsilon$ where N_D^+ is the ionized donor density of the surrounding semiconductors) and electronic transport (continuity and momentum conservation) equations. This solution provides an initial electric field value for the FDTD simulation. At steady state, Maxwell equations simplify to

$$\nabla \times \vec{E}^{\mathrm{dc}} = 0 \quad (5)$$

$$\nabla \times \vec{H}^{dc} = J_v^{\mathrm{dc}}. \quad (6)$$

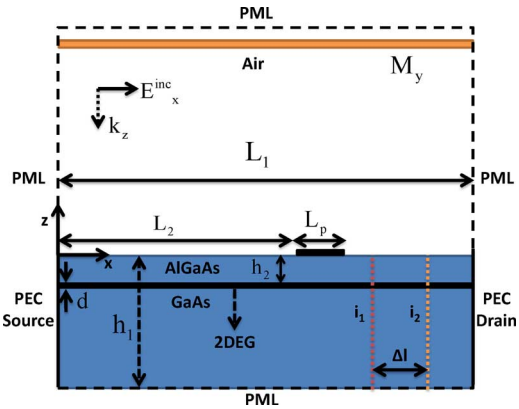

Fig. 1. 2-D structure simulated by the global modeling technique (figure not to scale).

Considering (6), it is suggested that the initial value of the magnetic field is introduced by the presence of $\vec{J}_v^{\,\mathrm{dc}}$. Therefore, the magnetic field will be initiated properly by implementing the steady state current density inside the FDTD code.

As the initialization process ends, an ac excitation is applied. By defining total electric $\vec{E}^{\,\mathrm{total}} = \vec{E}^{\,\mathrm{dc}} + \vec{E}^{\,\mathrm{ac}}$ and magnetic $\vec{H}^{\,\mathrm{total}} = \vec{H}^{\,\mathrm{dc}} + \vec{H}^{\,\mathrm{ac}}$ fields and using Maxwell equations, it is concluded that

$$\frac{\partial \vec{E}^{\,\mathrm{total}}}{\partial t} = \frac{1}{\varepsilon}\left(\nabla \times \vec{H}^{\,\mathrm{ac}} + \vec{J}_v^{\,dc} - \vec{J}_v^{\,\mathrm{total}}\right) \tag{7}$$

$$\frac{\partial \vec{H}^{\,\mathrm{total}}}{\partial t} = -\frac{1}{\mu}\nabla \times \vec{E}^{\,\mathrm{total}} \tag{8}$$

where $\vec{J}_v^{\,\mathrm{total}}$ is calculated by the device modeler after the ac excitation is applied. Therefore, the total electric and magnetic fields are updated at each time step by solving (8)–(9). These new values are fed to the device simulator to update the total current density at the same time step. Next, the updated total current density is used in the full wave solver to revise the fields at the following time step. This process continues until the set of equations satisfy each other self-consistently and the simulation becomes stable. A more detailed description of global modeling can be found in [25] and [26].

D. Simulated Plasmonic Structure and the Simulation Details

The 2-D schematic of the simulated active plasmonic structure is shown in Fig. 1. It is consisted of a hetero-structure (AlGaAs/GaAs) of thickness $h_1 = 7.5$ μm which is represented as a dielectric with $\varepsilon_r = 12.6$. Furthermore, a 2DEG layer of thickness $d = 20$ nm is assumed at $h_2 = 80$ nm underneath the surface. Ohmic contacts (named drain and source herein) at the device terminals are approximated as Perfect Electric Conductors (PECs) with fixed charge densities and very high electrical conductivities ($\approx 10^{10}$ S/m). This assumption is valid in most of the practical semiconductor devices due to very high surface recombination velocities at the contacts with excessive doping densities ($> 10^{17}$ cm^{-3}) [33]–[36]. An ac planar magnetic current sheet M_y, with a cell size thickness is considered in the top air section for the excitation. The magnetic current is oriented along $+y$ direction and is placed far enough away from the device, so that its evanescent modes do not reach the device. In this manner, only a plane wave hits the dielectric surface. The current source variations in time follow a sinusoidal shape with a single frequency $f = 1$ THz. Although the reported results are only for the single frequency of the incident sinusoidal wave, a wide band simulation can also be achieved using a Gaussian excitation pulse. Moreover, standard Perfect Match Layers (PML) developed by Berenger [37] are applied to the rest of the boundaries as depicted in Fig. 1. To reduce the numerical artifacts due to a finite spatial sampling of Maxwell equations, the PML losses along the direction normal to the boundary increase slowly from zero. To this end, PML layers with graded conductivities of a third-order polynomial profile and with the reflection error of 10^{-8} are employed [37]. It is assumed that the size of the device along y-axis is very large in comparison to the wavelength of the 2-D plasmons. Therefore, a 2-D FDTD simulation is adequate. The mesh size along x axis (Δx) is mainly controlled by the Debye length criteria $(\Delta x < \sqrt{\varepsilon k_B T/n_v})$ inside the semiconductor simulator and the wavelength criteria ($\lambda_p/10$ where λ_p is the 2-D plasmon wavelength) within the EM solver [25]. This condition leads to $\Delta x \approx 10$ nm which ought to be applied inside both simulators. Within the FDTD code, the 2DEG is represented as an electric current source with one cell size thickness. This sets the minimum mesh size along z axis $(\Delta z_{\min} = d)$. In order to reduce the computational burden enforced by the small 2DEG thickness, a non-uniform mesh is employed along z direction. The maximum allowable mesh size along z $(\Delta z_{\max})$ is defined by the wavelength of the incident field λ inside the dielectric. The maximum allowable simulation time step Δt is primarily defined by the Courant-Friendrichs-Lewy stability condition [37]. Taking this constraint into account, Δt becomes in the order of 10^{-17} s. Here, a 1-D solution of the transport equation is performed. This does not affect the accuracy of our analysis since electron movement in the z direction is restricted by the quantum confinement that exists inside the hetero-structure.

Appropriate boundary conditions are required to solve continuity and Poisson equations. To this end, charge densities of the 2DEG end nodes are fixed to their equilibrium value. This means that the ohmic contacts do not allow any charge density variations at their adjacent points. Inside the biased structure, the node placed at the source contact is grounded while the one at the drain is connected to the external bias voltage V_{ds}.

In order to excite the 2-D plasmons inside the 2DEG, a PEC section with one cell size thickness is placed on the top surface of the device $(z = 0)$ at $x = L_2$. Its length has been chosen to be very small compared to the wavelength of the radiating mode in the air. This PEC section represents thin metallic gratings that are mostly placed adjacent to the 2DEG layer. The gratings are frequently employed to excite 2-D plasmons by the incident wave diffraction. Hereafter, this thin metal is called plasmon launcher. The distance between the 2DEG and the plasmon launcher should be chosen appropriately so that a substantial amount of the diffracted wave couples to the 2DEG layer.

III. Results and Discussion

In this section, the described full wave simulator is employed to characterize the 2-D plasmon propagation along the detailed

hetero-structure under different bias voltages at a single frequency $f = 1$ THz. This frequency is chosen arbitrarily and the analysis is applicable at different frequencies. Herein, the surface charge density of the 2DEG layer is assumed $n_0 = 10^{11}$ cm^{-2}. Moreover, the length of the simulated device is $L_1 = 4$ μm (see Fig. 1). In this paper, the low field mobility of the hetero-structure is considered by the transport parameters $\tau_m = 1$ ps and $m^* = 0.063m_0$, where m_0 is the electron rest mass. The corresponding electron mobility is accessible even at 200 K [38]. In order to excite the SWCs, a plasmon launcher with length $L_p = 100$ nm is placed in the middle of the structure ($L_2 = 1.95$ μm) in the close proximity of the 2DEG layer at the top surface of the semiconductor.

In order to separate the SWCs excited at the plasmon launcher from the other field values such as the transmitted time varying field, two different simulations have been performed. First, the plasmon launcher is placed on the surface of the structure and the simulation is performed until a specific time step t_1. Next, a similar simulation is executed as the plasmon launcher is removed. Afterwards, the respective field values computed in the simulations are subtracted from each other.

A. 2-D Plasmon Propagation Inside an Unbiased Hetero-Structure

As previously presented in [7] and [30], 2-D plasmons propagate along unbiased conductors with propagation constants

$$\gamma = \pm\frac{j}{2a}\sqrt{\omega^4 - \frac{\omega^2}{\tau_m^2} - \frac{2j\omega^3}{\tau_m} + \frac{4a^2\omega^2\varepsilon_r}{c^2}}, \quad a = \frac{n_0 q^2}{4\varepsilon m^*} \tag{9}$$

where, $\omega = 2\pi$f and c are angular frequency and the speed of light in the vacuum, respectively. In the calculation of the dispersion relation (9), wave function (refer to [39] for the definition) of the plasmonic mode is considered as

$$\psi = \begin{cases} \phi_1 \exp(j\omega t - \gamma x - \delta z), & z \geq 0 \\ \phi_2 \exp(j\omega t - \gamma x + \delta z), & z < 0 \end{cases} \tag{10}$$

where γ is the complex propagation constant. Real (α) and imaginary (β) parts of γ are called attenuation and phase constants, respectively.

Inserting the 2DEG layer charge density and the transport parameters (including the momentum relaxation time) into (9), it is calculated that $\alpha_{1,2} = \pm 26.9$ dB/μm, $\beta_{1,2} = \pm 19.5$ rad/μm and the 2-D plasmons wavelength $(\lambda_p = 2 \times \pi/|\beta_{1,2}|)$ is 322 nm.

In Fig. 2(a), the electric field distribution of the 2-D plasmons in the proximity of the 2DEG layer calculated by the numerical solver, in the time step t_1 is depicted. As shown, SWCs are excited as a result of the incident wave diffraction at the plasmon launcher. It is also observed that the SWCs are facing large attenuations due to the electron scatterings as moving in $\pm x$ directions. In Fig. 2(b), the x component of the electric field (at $z = -h_2$) of the SWCs inside the unbiased hetero-structure is depicted. As illustrated, the numerical technique has calculated the 2-D plasmon propagation constant nearly equal to the

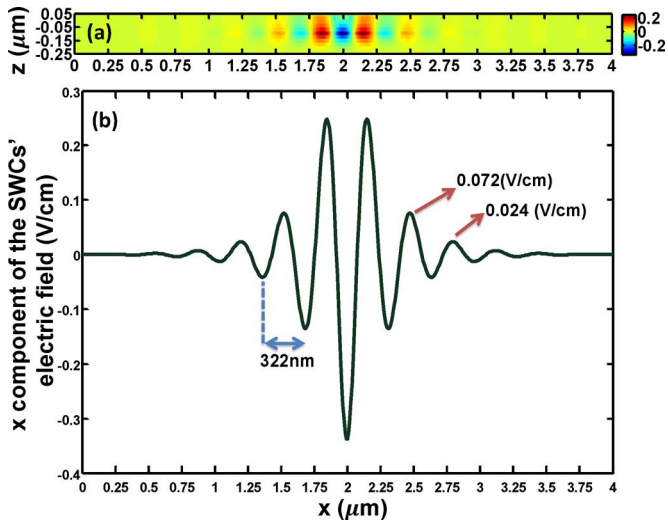

Fig. 2. SWCs' x-component of the electric field: (a) distribution close to the 2DEG layer and (b) variations at $z = -h_2$ are illustrated. The SWCs' attenuation constant is approximated $\pm$ 29.5 dB/μm. The SWCs' phase constants are estimated as $\pm$19.6 rad/μm.

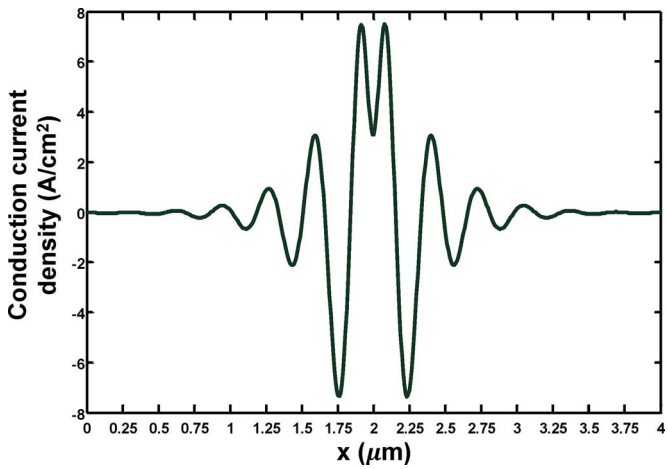

Fig. 3. The conduction current density variations due to the SWCs originated from the plasmon launcher at $z = -h_2$ are shown.

values estimated by the analytical model (9). The small deviation of the attenuation constant from the value predicted in (9) can be partly due to the presence of the ohmic contacts that are not considered by the analytical model. Here, the accuracy of the attenuation constant calculation has been improved using the technique detailed in Appendix I.

In Fig. 3, the conduction current variations (J_v) at $z = -h_2$ are depicted. This physical property can be useful in the design of plasmonic detectors with a specific responsivity. By choosing appropriate device length, channel properties and plasmon launcher size, the design of an efficient THz non-resonant plasmonic detector is possible. As shown in Fig. 3, the electrons are accelerated and decelerated at specific locations that correspond to the maximum magnitudes of the electric field.

B. 2-D Plasmon Propagation Inside a Biased Hetero-Structure

As previously proved analytically [30], the symmetrical 2-D plasmons inside the unbiased 2DEG with the dispersion relation

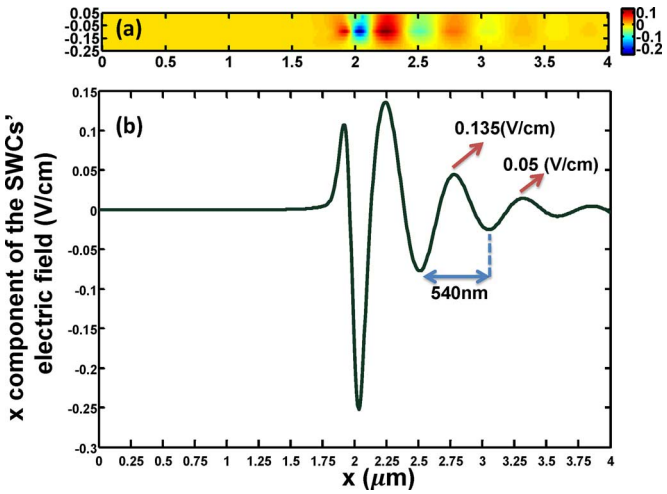

Fig. 4. SWCs' x-component of the electric field: (a) distribution next to the 2DEG layer and (b) variations at $z = -h_2$ are depicted. The SWCs' attenuation and phase constants are approximated as 15.9 dB/μm and 11.6 rad/μm, respectively.

defined in (9) split into four asymmetrical modes. The propagation constant of these modes are

$$A_1\gamma^4 + A_2\gamma^3 + A_3\gamma^2 + A_4\gamma + A_5 = 0 \tag{11}$$

where

$$\begin{aligned} A_1 &= v_0^4, \quad A_2 = -\frac{2v_0^3}{\tau_m} - 4j\omega v_0^3 \\ A_3 &= -6\omega^2 v_0^2 + \frac{v_0^2}{\tau_m^2} + \frac{6j\omega v_0^2}{\tau_m} + 4a^2 \\ A_4 &= 4jv_0\omega^3 + \frac{6v_0\omega^2}{\tau_m} - \frac{2jv_0\omega}{\tau_m} \\ A_5 &= \omega^4 - \frac{\omega^2}{\tau_m^2} - \frac{2j\omega^3}{\tau_m} + \frac{4a^2\omega^2\varepsilon_r}{c^2}. \end{aligned} \tag{12}$$

In (12), v_0 is the electron average drift velocity inside the biased hetero-structure.

Here, the bias voltage $V_{\rm ds} = 143$ mV is applied onto the ohmic contacts. This voltage establishes the electric field $E_0 = 360$ V/cm inside the device. Considering the linear relation between the electron average velocity and the electric field ($v_0 = (q\tau_m)/(m^*) \times E_0$), the electron velocity becomes $v_0 \approx 10^7$ cm/s. Using (11) and (12), it is concluded that the plasmonic modes propagating opposite to the electron drift stream suffer from very high attenuations compared to ones moving parallel to it. From (11), it is calculated that the $+x$ going plasmonic mode inside the biased structure propagates with $\alpha_1' = 14.7$ dB/μm, $\beta_1' = 12$ rad/μm and the wavelength 524 nm. On the other hand, the mode propagating in the opposite direction $(-x)$ yields the attenuation constant $\alpha_2' = 39.9$ dB/μm. Due to the large attenuation constant of the $-x$ going SWC, this specific mode is not excited as will be reported in the following.

In Fig. 4(a), the SWC electric field distribution in the proximity of the 2DEG layer inside the biased hetero-structure at time t_1 is depicted. In contrast to the unbiased device [Fig. 2(a)], the 2-D plasmons are propagating only in one direction $(+x)$. In Fig. 4(b), the x-component of the SWC electric field at $z = -h_2$ is depicted. As illustrated, there exist a slight difference between the phase constant of the plasmonic mode computed by the analytical method (12 rad/μm) and the one obtained from the numerical techniques (11.6 rad/μm). This alteration is by virtue of the wideband-gap semiconductor thickness consideration inside the full wave simulator. As expected, the bias field has caused large changes in the phase constant of the plasmonic mode. Besides, the $-x$ going plasmonic mode has not been excited due to the large attenuations. Considering these results, it seems that the steering of the 2-D plasmons can effectively become possible by applying bias voltage along the plasmonic waveguide.

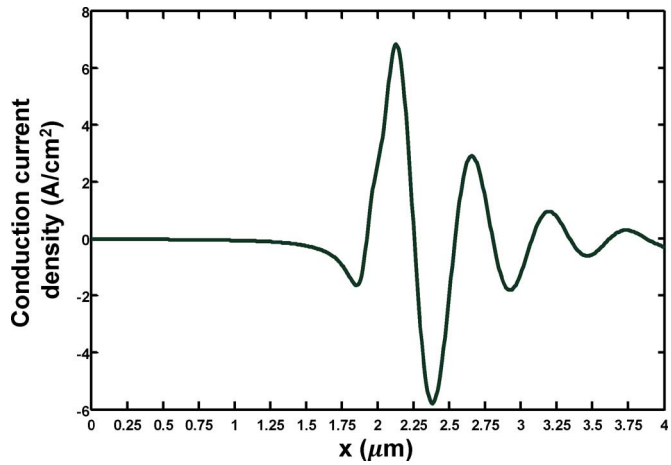

Fig. 5. SWCs' conduction current density variations at $z = -h_2$ is illustrated.

In Fig. 5, the variations of the 2-D plasmon conduction current at $z = -h_2$ are shown.

C. 2-D Plasmon Reflection From Ohmic Contacts Inside a Biased Hetero-Structure

To present the capabilities of the developed numerical technique compared to the analytical model, the 2-D plasmon reflections from ohmic contacts of the biased structure is analyzed. To this end, the plasmon launcher is considered closer to the drain contact ($L_2 = 3$ μm) compared to the previous case of study. This enables the excited surface waves to reach the contact before its amplitude becomes almost equal to zero. Fig. 6. depicts the variations of the x component of the electric field inside the biased hetero-structure. As expected, the $+x$ moving surface waves are originated from the launcher while high attenuations prevent any plasmon generation with the opposite direction of propagation. As illustrated in Fig. 6, the phase constant of the dominant mode along the electron gas layer has not been changed. Considering the magnitude of the electric field component at the proximity of the drain contact, interesting changes in the field distribution are observed. As depicted in the inset of the Fig. 6., the surface wave does not follow the wave function of the $+x$ going mode strictly next to the contact. This is due to the excitation of higher order evanescent modes or possibly the $-x$ moving plasmonic modes.

IV. Controlling the Wave Properties of 2-D Plasmons by Changing the Bias Voltage

Commonly, the charge densities of the 2DEG layers of hetero-structures are controlled by implementing a gate above the wideband gap semiconductor (top-gate) or beneath the

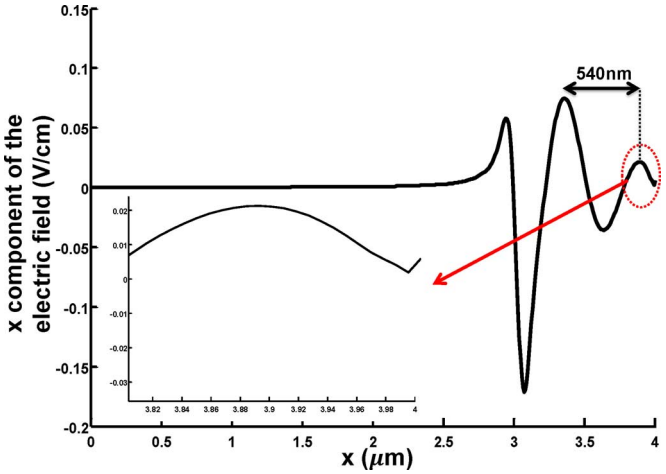

Fig. 6. Variations of the x-component of the electric field (V/cm) at $z = -h_2$ is depicted. The location of the plasmon launcher is chosen intentionally to observe the wave reflections from the drain. The inset portrays the field value changes next to the drain contact at $x = 4$ μm.

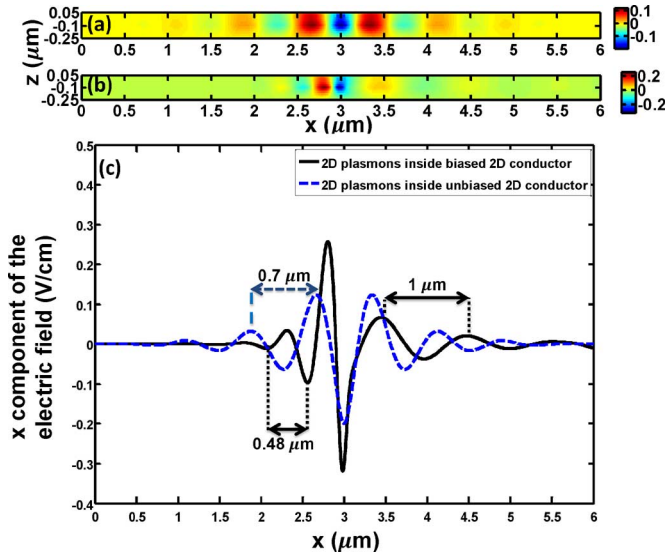

Fig. 7. (a), (b) Distribution of the "x"-component of the electric field next to the 2DEG layer of the unbiased and the biased hetero-structure are shown, respectively. (c) x-component of the electric field variations at $z = -h_2$ inside the device under different bias conditions is shown. The approximated attenuation constant inside the unbiased structure is 14.7 dB/μm. The $+x$ and $-x$ mode attenuation constants of the plasmons inside the biased device are 9.5 and 30.4 dB/μm, respectively.

substrate (back-gate). In this manner, the designer can simultaneously optimize the plasmonic circuit by changing the gate and the drain-source voltages. Here, the dependency of the plasmon properties on the 2DEG layer charge density is considered. To this end, the numerical simulator is employed to simulate the described structure as the electron density of the 2DEG layers has been increased to a new value $n_0' = 2 \times 10^{11}$ cm^{-2}.

Using (9), it is expected that the unbiased hetero-structure can guide plasmons with $\alpha_{1,2} = \pm 13$ dB/μm and $\beta_{1,2} = \pm 10$ rad/μm. However, the plamonic modes will divide into asymmetrical modes as the electrons are accelerated by an external bias field with an average electron velocity $v_0 \approx 10^7$ cm/s. The mode that propagates in $+x$ direction attains $\alpha_1' = 9.5$ dB/μm and $\beta_1' = 7.6$ rad/μm as the other mode which travels against the electron drift stream has $\alpha_2' = -26.9$ dB/μm and $\beta_2' = -15$ rad/μm.

In the full wave simulation, the device length and the surface charge density of the 2DEG have been increased to $L_1 = 6$ μm and $n_0' = 2 \times 10^{11}$ (cm^{-2}) as other specification are kept similar to the previous structure. In order to accelerate the electrons with the average velocity $v_0 = 10^7$ cm/s, the applied voltage has been augmented to $V_{\rm ds} = 215$ mV.

A. Surface Wave Excitation Using a Single Plasmon Launcher

Here, a metallic layer is considered in the middle of the simulated structure surface ($L_2 = 2.95$ μm to excite the plasmons. Fig. 7(a) and (b) display the ac electric field distribution of the 2-D plasmons calculated by the global modeling technique. As depicted in Fig. 7(a), the 2-D plasmons are propagating in the $\pm x$ directions symmetrically. As the bias voltage is applied onto the contacts, asymmetric 2-D plasmons are excited in the $+x$ and $-x$-directions [see Fig. 7(b)]. The x-component of the ac electric field at $z = -h_2$ is presented in Fig. 7(c) as $V_{\rm ds} = 0$ and 215 mV. As depicted, the numerical solver has calculated the propagation constants of the plasmonic modes equal to ± 9 rad/μm as $V_{\rm ds} = 0$, and 6.3, -13.1 rad/μm as $V_{\rm ds} = 215$ mV. Comparing the results attained from the analytical and the numerical techniques, it is understood that there exists a difference (about ten percent) between the outcomes which is due to the consideration of the wideband-gap semiconductor thickness

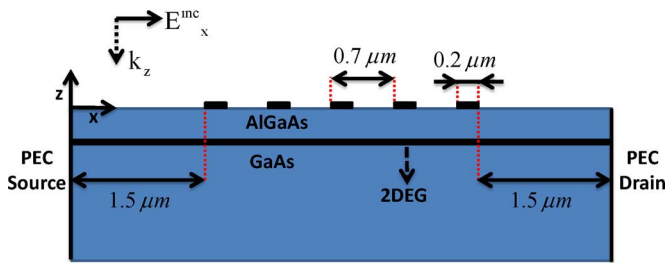

Fig. 8. Schematic of the simulated hetero-structure as the periodic grating is presented on the device surface.

inside the full wave simulator. As illustrated in Fig. 7(c), the wavelength of the $+x$ moving 2-D plasmons has been increased about 30% after applying the bias field. As demonstrated, the 2-D plasmonic mode that is allowed to propagate in the $-x$ direction has also been excited in contrast to the previous example. Therefore, the gate control voltage has helped to excite new plasmonic modes inside the device by doubling the electron gas charge density.

B. Plasmon Excitation Using a Metallic Grating

Here, the wave propagation along the 2DEG in the presence of a periodic grating is investigated. To this end, five periods of the PEC layer with length 0.2 μm employed. The arrangement of the grating on the device top surface is detailed in Fig. 8. The period of the grating (0.7 μm) is chosen equal to the wavelength of the plasmons inside the unbiased structure.

Fig. 9(a), (b) depict the ac electric field distributions along the electron gas layer as $V_{\rm ds} = 0$ and 215 mV, respectively. As presented in Fig. 9(a), (b), the surface waves are launched along the hetero-structure in both conditions. In Fig. 9(c), the variations of the electric field component are illustrated. As described in Fig. 9(c), the plasmonic mode with wavelength 0.7

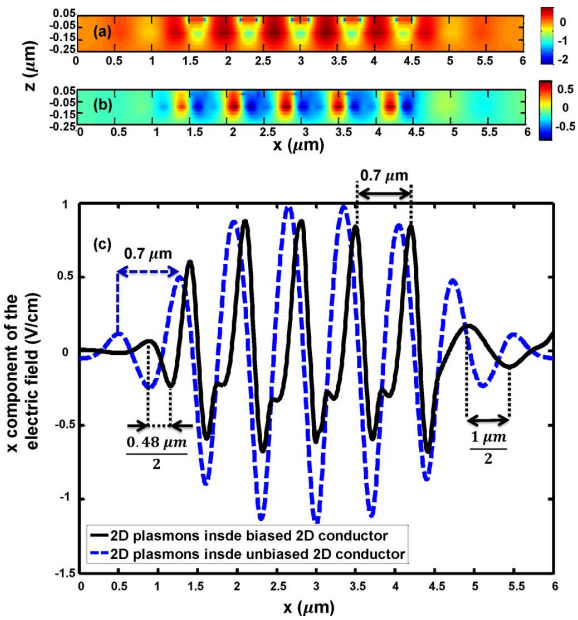

Fig. 9. (a), (b) Distribution of the "x" component of the electric field next to the 2DEG layer with the periodic grating under different bias conditions are shown. (c) x-components of the electric field variations at $z = -h_2$ inside the device as $V_{\rm ds} = 0$ and 215 mV are shown.

μm is uniformly launched along the electron gas inside the unbiased structure. However, the 2-D plasmons are weakly excited as the bias voltage is applied between the contacts. As presented, the $+x$ and $-x$ moving surface waves are excited inside the biased structure due to the diffraction of the incident wave at the periodic metallic grating. Due to the mismatch between the grating period and the plasmonic mode wavelengths, the plasmon launcher is performing inefficiently. Non-sinusoidal distribution of the electric field at locations between the periodic gratings is because of the summation of the different modes excited at the edges of neighboring metals. The field deviations from the $+x$ moving mode wave function discussed in Section III-C, are also depicted in Fig. 9(c) at the vicinity of the drain contact ($x = 6$ μm).

V. Conclusion

A full wave simulation technique is employed to analyze novel active plasmonic devices. The simulator solves Maxwell and the moments of Boltzmann equations numerically in a self-consistent manner. The effectiveness of this method is presented by characterizing 2-D plasmon propagation along the two dimensional electron gas layer of a hetero-structure under different bias conditions. Using this technique, vast variations in the plasmon properties originating from the biasing of the hetero-structure are reported. It is observed that the 2-D plasmons propagating against the electron drift motion face larger attenuations compared to the ones moving in the same direction. The analysis has been performed inside 2DEG layers with different charge densities to investigate the gating effects on the 2-D plasmon characteristics. It is concluded that new plasmonic modes can be excited by applying various bias voltages onto the device. This idea can help the designers to fabricate novel plasmonic devices such as switches and modulators. This numerical technique can also be useful in the modeling of available THz plasmonic detectors and sources.

Appendix

In order to calculate the plasmon attenuation constant α accurately, the following method is pursued. First, the x components of the Poynting vector at each grid point of two integration lines at an arbitrary time step t_1 are calculated $(E_y \times H_z)$. The locations of the integration lines should be chosen appropriately to represent a unique mode. This has been considered while choosing the integration lines i_1 and i_2 (see Fig. 1). Afterward, numerical integrations along the lines i_1 and i_2 on the computed power fluxes are performed. Thus, the transmitted power $P(t)$ handled by the specific plasmonic mode at time t_1 is obtained. This process is similarly repeated in the following time steps until a period of the incident field $(T = 1/f)$. Next, the time average transmitted power at each integration line is estimated as

$$P_{\rm avg}^{i_1,i_2} = \frac{1}{T}\sum_{t=t_1}^{t=t_1+T}[\Delta t \times P^{i_1,i_2}(t)]. \tag{13}$$

In this manner, the plasmon attenuation constant of each specific mode is calculated as

$$\alpha = \frac{1}{2\Delta l}\ln\left(\frac{P_{\rm avg}^{i_1}}{P_{\rm avg}^{i_2}}\right) \tag{14}$$

where Δl is the distance between i_1 and i_2.

Acknowledgment

One of the authors, M. A. Khorrami, would like to thank Dr. J. S. Ayubi-Moak with Synopsys, Inc., for fruitful discussion and assistance.

References

[1] L. Ju, B. Geng, J. Horng, C. Girit, M. Martin, Z. Hao, H. A. Bechtel, X. Liang, A. Zettl, Y. R. Shen, and F. Wang, "Graphene plasmonics for tunable terahertz metamaterials," *Nature Nanotechnol.*, vol. 6, pp. 630–634, Sep. 2011.

[2] L. Ji and V. V. Varadan, "Fishnet metastructure for efficiency enhancement of a thin film solar cell," *J. Appl. Phys.*, vol. 110, p. 043114, Aug. 2011.

[3] M. Lee and M. C. Wanke, "Searching for a solid state technology," *Science*, vol. 316, pp. 64–65, Apr. 2007.

[4] S. A. Maier, *Plasmonics: Fundamentals and Applications*. New York, NY, USA: Springer, 2007.

[5] Z. Fu, Q. Gan, Y. J. Ding, and F. J. Bartoli, "From waveguiding to spatial localization of THz waves within a plasmonic metallic grating," *IEEE J. Sel. Topics Quantum Electron.*, vol. 14, no. 2, pp. 486–490, Mar./Apr. 2008.

[6] W. Zhu, A. Agrawal, A. Cui, G. Kumar, and A. Nahata, "Engineering the propagation properties of planar plasmonic terahertz waveguides," *IEEE J. Sel. Topics Quantum Electron.*, vol. 17, no. 1, pp. 146–153, Jan./Feb. 2011.

[7] F. Stern, "Polarizabilty of a two-dimensional electron gas," *Phys. Rev. Lett.*, vol. 18, no. 14, pp. 546–548, Apr. 1967.

[8] M. Dyakonov and M. Shur, "Detection, mixing, and frequency multiplication of Terahertz radation by two-dimensional electron fluid," *IEEE Trans. Electron Devices*, vol. 43, no. 3, pp. 380–387, Mar. 1996.

[9] P. J. Burke, I. B. Spielman, J. P. Eisenstein, and L. N. Pfeiffer, "High frequency conductivity of the high-mobility two-dimensional electron gas," *App. Phys. Lett.*, vol. 76, no. 6, pp. 745–747, Feb. 2000.

[10] M. A. Khorrami and S. El-Ghazaly, "2-D plasmon propagation inside a two-dimensional electron gas layer with a low loss metallic gate," in *IEEE Photon. Conf. (IPC)*, Sep. 2012, pp. 895–896.

[11] A. K. Geim and K. S. Novoselov, "The rise of graphene," *Nature*, vol. 6, pp. 183–191, Mar. 2007.
[12] R. Alaee, M. Farhat, C. Rockstuhl, and F. Lederer, "A perfect absorber made of a graphene micro-ribbon metamaterial," *Opt. Express*, vol. 20, no. 27, p. 28017, Dec. 2012.
[13] W. F. Andress, H. Yoon, K. Y. M. Yeung, L. Qin, K. West, L. Pfeiffer, and D. Ham, "Ultra-subwavelength two-dimensional plasmonic circuits," *Nano Lett.*, vol. 12, pp. 2272–2277, Apr. 2012.
[14] M. Nakayama, "Theory of surface waves coupled to surface cariers," *J. Phys. Soc. Jpn.*, vol. 36, no. 2, pp. 393–398, Sep. 1974.
[15] B. Sensale-Rodrigues, L. Liu, P. Fay, D. Jena, and H. Grace, "Power amplification at THz via plasma wave exciation in RTD-gated HEMTs," *IEEE Trans. THz Sci. Technol.*, vol. 3, no. 2, Mar. 2013.
[16] W. Knap, J. Lusakowski, T. Parenty, S. Bollaert, A. Cappy, V. V. Popov, and M. S. Shur, "Terahertz emission by plasma waves in 60 nm gate high electron mobility transistors," *Appl. Phys. Lett.*, vol. 84, pp. 2331–2333, Mar. 2004.
[17] T. Otsuji, T. Watanabe, S. A. B. Tombet, A. Satou, W. M. Knap, V. V. Popov, M. Ryzhii, and V. Ryhzhii, "Emission and detection of terahertz radiation using two-dimensional electrons in III-V semiconductors and graphene," *IEEE Trans. THz Sci. Technol.*, vol. 3, no. 1, Jan. 2013.
[18] H. Saxena, R. E. Peale, and W. R. Buchwald, "Tunable two-dimensional plasmon resonances in an InGaAs/InP high electron mobility transistor," *J. Appl. Phys.*, vol. 105, pp. 113101–113106, June 2009.
[19] V. V. Popov, D. M. Ermolaev, K. V. Maremyanin, N. A. Maleev, and V. E. Zemlyakov, "High-responsivity terahertz detection by on-chip InGaAs/GaAs field-effect-transistor array," *Appl. Phys. Lett.*, vol. 98, pp. 153504(1)–153504(3), Apr. 2011.
[20] M. A. Khorrami, S. El-Ghazaly, S. Q. Yu, and H. Naseem, "Compact terahertz surface plasmon switch inside a two dimensional electron gas layer," in *Int. IEEE Microw. Symp.*, Montreal, Canada, Jun. 2012.
[21] A. R. Davoyan, V. V. Popov, and S. A. Nikitov, "Tailoring terahertz near-field enhancement via two-dimensional plasmons," *Phys. Rev. Lett.*, vol. 108, p. 127401, Mar. 2012.
[22] G. R. Aizin and G. C. Dyer, "Transmission line theory of collective plasma excitation in periodic two-dimensional electron systems: Finite plasmonic crystals and Tamm states," *Phys. Rev. B*, vol. 86, Dec. 2012, Art. No. 235316.
[23] H. Marinchio, J. F. Millithaler, C. Palermo, L. Varani, L. Reggiani, P. Shiktorov, E. Starikov, and V. Gruzinskis, "Plasma resonances in a gated semiconductor slab of arbitrary thickness," *Appl. Phys. Lett.*, vol. 98, p. 203504, May 2011.
[24] J. Mateos and T. Gonzalez, "Plasmsa enhanced terahertz rectification and noise in InGaAs HEMTs," *IEEE Trans. THz Sci. Technol.*, vol. 2, no. 5, pp. 562–569, Sep. 2012.
[25] M. A. Alsunaidi, S. M. S. Imtiaz, and S. El-Ghazaly, "Electromagnetic wave effects on microwave transistors using a full-wave high-frequency time-domain model," *IEEE Trans. Microw. Theory Techn.*, vol. 44, no. 6, pp. 779–808, Jun. 1996.
[26] R. O. Grondin, S. El-Ghazaly, and S. Goodnick, "A review of global modeling of charge transport in semiconductors and full-wave electromagnetics," *IEEE Trans. Microw. Theory Techn.*, vol. 47, no. 6, pp. 817–829, June 1999.
[27] K. J. Willis, S. C. Hagness, and I. Knezevic, "Terahertz conductivity of doped silicon calculated using the ensemble Monte Carlo/finite-difference time-domain simulation technique," *Appl. Phys. Lett.*, vol. 96, p. 062106, Feb. 2010.
[28] N. Sule, K. J. Willis, S. C. Hagness, and I. Knezevic, "Simulation of carrier dynamics in graphene on a substrate at terahertz and mid-infrared frequencies," in *12th Int. Conf. on Numerical Simulation of Optoelectronic Devices (NUSOD)*, Shanghai, China, Aug. 2012, pp. 79–80.
[29] M. A. Khorrami, S. El-Ghazaly, S. Q. Yu, and H. Naseem, "Analytical modeling of THz wave propagation inside ungated two dimensional electron gas layers," in *Int. IEEE Microw. Symp.*, Baltimore, MD, USA, Jun. 2011.
[30] M. A. Khorrami, S. El-Ghazaly, S. Q. Yu, and H. Naseem, "THz plasmon amplification using two-dimensional electron-gas layers," *J. Appl. Phys.*, vol. 111, p. 094501, May 2012.
[31] S. M. Sze and K. K. Ng, *Physics of Semiconductor Devices*. , New Jersey: John Wiley & Sons, 2007.
[32] K. S. Yee, "Numerical solution of initial boundary value problems involving Maxwell's equation in isotropic media," *IEEE Trans. Antennas Propag.*, vol. AP-14, pp. 302–307, May 1966.
[33] V. Palankovski and R. Quay, *Analysis and Simulation of Heterostructure Devices*. Vienna, Austria: Springer-Verlag, 2004.
[34] C. M. Snowden, "Semiconductor device modeling," *Rep. Progr. in Phys.*, vol. 48, no. 2, p. 223, Feb. 1985.
[35] F. J. Crowne, "Contact boundary conditions and the Dyakonov–Shur instability in high electron mobility transistors," *J. Appl. Phys.*, vol. 82, no. 3, p. 1242, Aug. 1997.
[36] W. R. Calderón-Muñoz, D. Jena, and M. Sen, "Hydrodynamic instability of confined two-dimensional electron flow in semiconductors," *J. Appl. Phys.*, vol. 106, p. 014506, Jul. 2009.
[37] A. Taflove and S. C. Hagness, *Computational Electrodynamics: The Finite-Difference Time-Domain Method*, 3rd ed. Norwood, MA, USA: Artech House, 2005.
[38] L. Pfeiffer, K. W. West, H. L. Stormer, and K. W. Baldwin, "Electron motilities exceeding 10^7 $cm^2/V \cdot s$ in modulation-doped GaAs," *Appl. Phys. Lett.*, vol. 55, pp. 1888–1890, Aug. 1989.
[39] C. A. Balanis, *Advanced Engineering Electromagnetics*. Hoboken, NJ, USA: Wiley, 1989.

Mohammad Ali Khorrami (S'09) received B.S. degree in electrical engineering from Ferdowsi University of Mashhad, Mashhad, Iran, in 2004, the M.S. degree in electrical engineering from Tehran Poly-technique University, Tehran, Iran, in 2008, and is currently working toward the Ph.D. degree in electrical engineering from the University of Arkansas, Fayetteville, AR, USA.

From 2005 to 2007, he was a Research Assistant with the Electromagnetic Compatibility Laboratory of Tehran Poly-technique University, Tehran, Iran. From 2009, he is a Research Assistant with the Electrical Engineering Department of the University of Arkansas, USA. His research interest includes the design and modeling of terahertz plasmonic devices, electrical characterization of microwave devices, electromagnetic compatibility and signal/power integrity for high-speed digital systems.

Mr. Khorrami has been selected to receive Young Scientist Award by International Union of Radio Science (URSI) General Assembly in 2008, Chicago, IL, USA. He was the recipient of the IEEE EMC Society grant to attend the annual IEEE International Symposium on EMC in 2013.

Samir M. El-Ghazaly (S'84–M'86–SM'91–F'01) received the B.S. and M.S.(Honos.) degrees in electronics and communications engineering from Cairo University, Cairo, Egypt, in 1981 and 1984, respectively, and the Ph.D. degree in electrical engineering from the University of Texas at Austin, Austin, TX, USA, in 1988.

He joined Arizona State University as an Assistant Professor in the Department of Electrical Engineering, where he became Associate Professor in 1993, and Professor in 1998. From 2002 to 2007, he was a professor and head of the Department of Electrical and Computer engineering at the University of Tennessee, Knoxville, TN, USA. He has been distinguished professor of the Electrical Engineering Department of University of Arkansas, Fayetteville, since 2007. From 2009, he served as an Electrical, Communications and Cyber Systems program and division director at the US National Science Foundation while retaining his academic position. His research interests include RF and microwave and millimeter-wave semiconductor devices, electromagnetic, and numerical techniques applied to MMICs radio-frequency nanotechnology devices. He has authored and co-authored over 200 research papers in refereed journals and proceedings.

Dr. El-Ghazaly is a member of Tau Beta Pi, Sigma Xi, and Eta Kappa Nu. He is an elected member of Commissions A and D, URSI. He has been a member of the Technical Program Committee for the IEEE Microwave Theory and Techniques Society (IEEE MTT-S) International Microwave Symposium (IMS) since 1991. He was the President of the IEEE's Microwave Theory and Techniques Society (MTT-S) in 2010.

Hameed A. Naseem received the B.Sc. (Hons.) and M.Sc. (Hons.) degrees in physics from Panjab University, Chandigarh, India, and the M.S. degree in physics, and Ph.D. degree in materials engineering science from Virginia Polytechnic Institute and State University, Blacksburg, VA, USA, in 1980 and 1984, respectively.

In 1984–1985., he was a Postdoctoral Research Associate at Southern Methodist University, Dallas, TX, USA. In 1985, he joined the University of Arkansas, Fayetteville, AR, USA, as an Assistant Professor, and was promoted to the rank of Associate Professor in 1990 and Full Professor in 1995, and is currently a Professor of Electrical Engineering. He has published over 100 research papers in refereed journals and proceedings. He has received three U.S. patents and several are pending.

Dr. Naseem has received numerous teaching and research awards including Texas Instruments Outstanding Faculty Award (1996), Haliburton Outstanding Teacher Award (1992), Philips Petroleum Company Outstanding Researcher Award (1994) and Arkansas Academy of Electrical engineering Outstanding Faculty Award (1988, 1993, and 1996). He is a member of Sigma Pi Sigma, Eta Kappa Nu, and Phi Beta Delta (International Scholars Honor Society).

Shui-Qing (Fisher) Yu (M'01) was born in Tianjian, China, in 1974. He received the B.S. and M.S. degrees in electronics from Peking University, China, in 1997 and 2000, respectively, and the Ph.D. degree in electrical engineering from Arizona State University (ASU), Tempe, AZ, USA, in 2005.

From 2005 to 2006, he was a Postdoctoral Research Associate in MBE Optoelectronics Group at ASU. From 2007 to 2008, he worked as an assistant research professor in Arizona Institute of Nano Electronics at ASU. Since 2008, he has been an Assistant Professor with the Electrical Engineering Department, University of Arkansas, Fayetteville, AR. He is the author of 40 journal papers and over 100 conference papers and holds one patent. His research interests include developing novel semiconductor optoelectronic devices such as lasers, photo detectors, THz devices, and renewable energy devices covering visible to far-infrared wavelength ranges by using novel III-V-Bi and SiGeSn alloys and advanced nanofabrication techniques.

Prof. Yu was a recipient of the IEEE Phoenix Chapter Society Award (2008) and the NSF Faculty Early Career Award (2012).